HHS Public Access

Author manuscript

Anal Chem. Author manuscript.

Signature of Antibody Domain-Exchange by Native Mass Spectrometry and Collision Induced Unfolding

Yasunori Watanabe[1,3,5], **Snezana Vasiljevic**[1], **Joel D. Allen**[3], **Gemma E. Seabright**[1,3], **Helen M. E. Duyvesteyn**[5], **Katie J. Doores**[4], **Max Crispin**[3,*], and **Weston B. Struwe**[1,2,*]

[1]Oxford Glycobiology Institute, Department of Biochemistry, University of Oxford, OX1 3QU, United Kingdom

[2]Chemistry Research Laboratory, Department of Chemistry, University of Oxford, OX1 3QZ, United Kingdom

[3]Biological Sciences & the Institute for Life Sciences, University of Southampton, SO17 1BJ, United Kingdom

[4]Department of Infectious Diseases, King's College London, SE1 9RT, United Kingdom

[5]Division of Structural Biology, University of Oxford, Wellcome Centre for Human Genetics, Roosevelt Drive, OX3 7BN, United Kingdom

Abstract

The development of domain-exchanged antibodies offers a route to high affinity targeting to clustered multivalent epitopes, such as those associated with viral infections and many cancers. One strategy to generate these antibodies is to introduce mutations into target antibodies to drive domain-exchange using the only known naturally-occurring domain-exchanged anti-HIV IgG1 antibody, 2G12, as a template. Here, we show that domain-exchange can be sensitively monitored by ion-mobility mass spectrometry and gas-phase collision induced unfolding. Using native 2G12 and a mutated form that disrupts domain-exchange such that it has a canonical IgG1 architecture (2G12 I19R), we show that the two forms can be readily distinguished by their unfolding profiles. Importantly, the same signature of domain-exchange is observed for both intact antibody and isolated Fab fragments. The development of a mass spectrometric method to detect antibody domain-exchange will enable rapid screening and selection of candidate antibodies engineered to exhibit this and other unusual quaternary antibody architectures.

Graphical Abstract

[*]**Corresponding Author**. weston.struwe@chem.ox.ac.uk (WBS) max.crispin@soton.ac.uk (MC).

ASSOCIATED CONTENT

Supporting Information

Supporting Information is available free of charge on the ACS Publications website. They include Figures S1 and S2 showing the IM-MS spectra of 2G12 and 2G12 I19R N-glycans and CIU data of B12, trastuzumab, 2G12 I19R and 2G12 charge states not presented in the main text.

Author Contributions

WS and MC conceived the project. YW, MC, and WS designed experiments. SV made key reagents. YW, JA and WS performed intact mass spectrometry experiments. HD completed statistical analyses. GS performed UPLC analysis. YW, MC and WS produced the first draft of the paper and all authors contributed to and approved of the final draft.

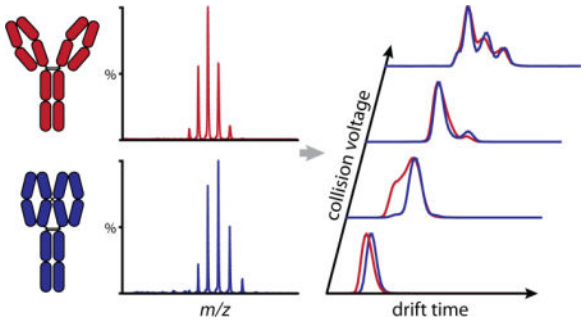

Antibodies (Ab) have emerged as the leading format for bio-therapeutics due to their fine target specificity and their ability to recruit immune effector functions[1]. Most immunoglobulin-based therapeutics are based on the IgG format whereby target recognition is mediated through the variable domains of the fragment antigen-binding (Fab) and the fragment crystallizable (Fc) domain mediates immune effector functions via complement activation and/or binding to cellular Fcγ receptors[2–4].

The Fc activity can be fine-tuned or silenced by both protein and glycan engineering[5–8]. In this way, therapeutic antibodies can be designed that either have minimal immunological effect or can exhibit elevated immune recruitment for maximal cell killing. In contrast, much less attention has been paid to exploring enhancing the target selectivity beyond that achieved by a natural Fab architecture. One approach to circumvent this limitation has been the development of bispecific antibodies (bsAb) where target selectivity is enhanced by Fabs of differing specificity[9–11]. A further under-explored architecture is the use of domain-exchanged IgG whereby the Variable domains from the two heavy chains (V_H and $V_{H'}$) are exchanged leading to a compact dual Fab[12]. This architecture was discovered during the epitope mapping of 2G12, an anti-body that is capable of neutralizing a broad range of human immunodeficiency virus (HIV) isolates (Figure 1A)[13]. This Ab is unusual in that the epitope consists of the dense cluster of N-linked glycans on the outer domain of the HIV attachment glycoprotein, gp120[13,14]. 2G12 specifically recognizes terminal Manα1-2Man-linked moieties predominantly found on $Man_8GlcNAc_2$ and $Man_9GlcNAc_2$[15–17]. Domain-exchange is critical for effective binding as the target glycans for the canonical Fab binding sites are only 20Å apart[15]. In addition, domain exchange may generate a new glycan binding surface at the $V_H/V_{H'}$ interface which further enhances binding[12,18].

Domain-exchange of 2G12 has been verified by X-ray crystallography of the isolated $(Fab)_2$ domain as well as size-exclusion chromatography, analytical ultracentrifugation and electron microscopy[12,18]. A single point mutation, I19R completely results in the undomain-exchanged, classical IgG format and X-ray crystallography of the resulting isolated Fab was shown to exhibit identical V_H/V_L structure compared to the parental domain-exchanged form[19] (Figure 1B). It has been suggested that domain-exchange architecture on antibodies could be used to target multivalent ligands in tumors and pathogens by providing binding specificities that go beyond the classical Fab paradigm. However, identifying domain-exchanged antibodies by aforementioned techniques is low-throughput and requires considerable amounts of protein.

Using native ion-mobility mass spectrometry (IM-MS), which separates ions not only by their mass-to-charge ratio but also by their three-dimensional shape, and collision induced unfolding (CIU), which activates selected ions prior to IM separation, we sought to explore whether domain-exchanged antibody architecture of 2G12 could be distinguished. Compared to other MS-based approaches, native MS maintains proteins in their intrinsically folded state and is an emerging method for biotherapeutic analysis[20–23]. IM-MS has proven useful to study thermal stability[24], dynamics[25,26], interactions[27] and biosimilarity[28] of intact monoclonal antibodies. CIU experiments utilize both collision activation to induce protein unfolding and IM separation which is based on the rotationally averaged collision cross section (CCS) of the ion[29–31]. CIU of protein complexes is an efficient tool to detect various protein features, including discriminating IgG glycosylation and disulfide bonding[32]. Additionally, native IM-MS has proven capable of charactering antibody drug conjugates, specifically assigning drug to antibody ratio of trastuxumab emtansine[33].

With antibodies at the forefront of biotherapeutics, a high-throughput analytical technique for the assessment of their structural properties is desirable[34]. Here we continue the development of IM-MS and CIU as an analytical technique, and show that gas-phase methods offer a route to rapid and sensitive screening of unusual quaternary architectures that arise from antibody engineering. We examine the CIU profiles of 2G12 and 2G12 I19R Abs and confirm that the specific foot-prints are determined solely by the domain-exchanged architecture of 2G12.

EXPERIMENTAL SECTION

Antibody Expression and Purification

Plasmids encoding antibody heavy and light chains of 2G12 and 2G12 I19R, b12 and trastuzumab were transiently expressed in HEK 293F cells at a density of 1×10^6 cells/ml. Transfection was done with a 1:2 construct ratio (heavy to light chain) and cells were grown for five days. Cells were pelleted and the supernatant was loaded onto a HiTrap Protein A column (GE Healthcare) using the manufacturers protocol. The binding buffer was 20 mM sodium phosphate pH 7.5 and the elution buffer was 0.1 M citric acid pH 3. Antibodies were immediately neutralized with 1 M Tris-HCl pH 9 prior to buffer exchange into PBS using a 50 kDa cut-off Vivaspin column (Sartorius). Antibodies were stored at 4°C until prior to analysis.

Enzyme-Linked Immunosorbent Assay

ELISAs were performed using 96-well Ni-NTA HisSorb plates (Qiagen). Plates were incubated overnight at 4 °C with 10 μg of HIV gp120, expressed as described[35]. Plates were washed four times with 0.5% PBS/Tween, and blocked with 5% skim milk/PBS for one hour at room temperature. Serial dilutions of 2G12 and 2G12 I19R antibodies in 5% skim milk/PBS were incubated for an hour. Unbound antibody was removed by washing as described above. Horse radish peroxidase conjugated anti-human goat IgG (ThermoFisher Scientific) was added at a 1:3000 dilution for one hour. The chromogen tetramethylbenzidine was added for 5 mins then neutralized using 2 M sulphuric acid. Absorbance was measured at 450 nm.

IdeS Expression and Purification

Recombinant IdeS was expressed in *E. coli* BL21 (DE3) cells. 500 ml of MagicMedia (Invitrogen) containing carbenicillin (100 μg/ml) was inoculated with the 12.5 ml of an overnight seed culture. Cells were grown at 30 °C with shaking at 300 rpm for 7 hours then at 25 °C for a further 24 hours. Cells were harvested by centrifugation at 4,000 g for 30 mins. Bacterial lysis was performed by sonication at 4 °C in a lysis buffer of 30 mM sodium phosphate, 300 mM NaCl, and pH 8. After centrifugation at 30,000 g for 40 mins the filtered supernatant was loaded onto a HisTrap column (GE Healthcare) with a binding buffer of 100 mM HEPES, 150 mM NaCl at pH 7.5. Sequential elutions of IdeS was performed using increasing concentrations of imidazole from 20 mM to 300 mM.

IdeS Cleavage

2G12 and 2G12 I19R were incubated for 2 hours at 37 °C with IdeS (IdeS to antibody ratio of 1:100) to generate intact Fc and Fab antibody fragments. IdeS was produced in-house.

Ion Mobility Mass Spectrometry and Collision Induced Unfolding

Samples were buffer exchanged into 200 mM ammonium acetate, pH 6.9 with Bio-Spin™ 6 columns (Bio-Rad). Additional desalting was accomplished by three sequential washes of 200 mM ammonium acetate using 50 kDa molecular weight cut-off (MWCO) centrifugal spin filters (GE Healthcare). Samples were diluted to 10 μM and analysed with a Synapt G2Si mass spectrometer (Waters, Manchester, UK). A nano-electrospray (nESI) ion source was used with gold-coated borosilicate glass capillaries prepared in-house. Instrument settings were as follows: capillary voltages, 1.4–1.8 kV; source temperature, 30 °C; sampling cone, 10 kV; trap DC bias, 20 V; trap gas flow, 5 ml/min; helium cell gas flow, 5 ml/min; IMS gas flow, 30 ml/min; trap wave velocity, 311 m/s; trap wave height, 4 V. Data acquisition and processing were carried out using MassLynx v4.11 and Driftscope version 2.8 software (Waters, Manchester, UK)

For CIU experiments, collision energy was applied in the trap region prior to IM. The collision voltage was increased from 4 to 200 V in 10 V increments. IM data were collected for 1 min at each collision voltage. Unfolding plots were created using PULSAR software, available from http://pulsar.chem.ox.ac.uk[36]. Mass fitter was utilized using the following parameters: mass = 150 kDa, Zavg = 24, Zwidth = 1.5, resolution = 900, and maximum intensity = 1. Experiments were grouped according to hierarchy based on collision voltages.

Drift time data were extracted using Driftscope version 2.8 (Waters, Manchester, UK), and statistical analysis was performed using python2.7 version of CIUSuite package[37]. Root-mean-squared-deviation (RMSD) values were calculated using CIUSuite stats and compare modules between 2G12 and 2G12 I19R variants.

Differential Scanning Calorimetry

Antibody samples were prepared at a concentration of 20 μM in 400 μl of phosphate buffered saline. DSC measurements were performed on a Malvern VP Capillary DSC (Malvern), with an unfolding temperature range of 30–110 °C.

Glycan Analysis

N-linked glycans were enzymatically cleaved from SDS-PAGE gels using PNGaseF prepared in-house. Released N-glycans were fluorescently labelled with 2-aminobenzoic acid (2-AA) for analysis by hydrophilic interaction chromatography ultra-high performance liquid chromatography (HILIC-UHPLC) with a Waters Acquity UPLC instrument, as previously described[38]. Glycan compositions were determined using traveling wave (TW) IM-MS measurements performed on a Synapt G2Si instrument (Waters, Manchester, UK). For each analysis 2 μl of sample were cleaned with a Nafion 117 membrane and directly infused by nano-electrospray ionization (nano-ESI) from gold-coated borosilicate glass capillaries as previously described[16,39]. Instrument settings were as follows: capillary voltage, 0.8–1.0 kV; sample cone, 100 V; extraction cone, 25 V; cone gas, 40 l/h; source temperature, 150 °C; trap collision voltage, 4–160 V; transfer collision voltage, 4 V; trap DC bias, 35–65 V; IMS wave velocity, 450 m/s; IMS wave height, 40 V; trap gas flow, 2 ml/min; IMS gas flow, 80 ml/min. Data was acquired and processed with MassLynx v4.1 and Driftscope version 2.8 software (Waters, Manchester, UK).

RESULTS AND DISCUSSION

Functional ELISA Assay to Characterise Domain-Exchange

Prior to IM-MS and CIU experiments, an ELISA assay was used to confirm the impact of each 2G12 antibody architecture on function. The monovalent I19R variant is able to recognize HIV gp120 monomers but with a lower affinity to the divalent domain-exchanged 2G12[15]. Wells were coated with gp120 (BG505 clade A strain) which has 24 N-glycosylation sites and binding was measured from serial dilutions of the antibodies. Expectedly, binding to gp120, which displays the oligomannose-type glycans of the 2G12 epitope[40–42] differs between 2G12 and 2G12 I19R (Figure 2). These data are consistent with the expected 2G12 and 2G12 I19R architectures were and that the material was suitable for subsequent MS experiments.

Differential scanning calorimetry of 2G12 and 2G12 I19R

Differential scanning calorimetry (DSC), a technique that measures unfolding in-solution due to heat denaturation, was used to explore the potential for different thermodynamic properties between 2G12 mAbs. DSC revealed that 2G12 I19R unfolded in the manner previously observed for typical IgG1 antibodies[43,44], with three transitions; first C_H2 domain unfolding (T_m = 61.0 °C), followed by Fab unfolding (T_m = 72.9 °C) and unfolding of the C_H3 domain (T_m = 86.0 °C) (Figure 3). The domain-exchanged 2G12 only yielded two transitions, with the first unfolding state occurring at 73.7 °C and the second at 86.0 °C. The C_H2 domain and the Fab region of 2G12 unfolds at the same temperature, possibly due to the domain-exchanged architecture, whilst the C_H3 domain un-folds at the same temperature as 2G12 I19R. Importantly DSC unfolding profiles can range significantly among typical IgGs[43,45] but these results point to different stability properties between 2G12 and 2G12 I19R.

Native Mass Spectrometry and Ion Mobility of 2G12 and 2G12 I19R

We next tested gas-phase separation of both antibodies by ion mobility MS. The native MS spectra of 2G12 and 2G12 I19R were characteristic of an intact folded IgG1 with charge states ranging between 22^+ to 26^+ (2G12) and 21^+ to 25^+ (2G12 I19R) (Figure 4A). The 2G12 charge-state distribution was slightly higher with 24^+ as the major charge state whereas for 2G12 I19R, the 23^+ charge state was foremost followed closely by 24^+. In principle, the difference in distribution of charge could be attributed to differences in available surface area (during electrospray desolvation) exhibited by undomain-exchanged (2G12 I19R) or domain-exchanged (2G12) Fab architectures. Interestingly, the IM drift times of 2G12 were greater between all charge states ($22–25^+$) which directly infers a larger CCS compared to the canonical undomain-exchanged IgG (2G12 I19R) architecture (Figure 4B). Although subtle, the intact MS analysis indicates differences exist between 2G12 and 2G12 I19R, however, these data alone are inconclusive to recognize domain-exchange among unknown IgGs.

Collision Induced Unfolding Signatures of Domain-Exchanged Antibodies

We next assessed CIU differences between 2G12 and 2G12 I19R (Figure 5). In a CIU experiment the unfolding of a protein (induced by increased collision voltages) is monitored as a function of drift time. The resulting 2-dimensinal data follow the progressive unfolding or change in size from the initial folded protein ion. The relative abundance of each transition is presented (Figure 5, **blue line**) over the course of each applied voltage. From the initial folded state, the CIU plot follows unfolded intermediates, sometimes referred to as transitions, and represents gas-phase stability of a protein complex.

The CIU profiles of 2G12 and 2G12 I19R 24^+ charge state revealed differences in gas-phase unfolding with 2G12 under-going its first unfolding transition at a lower collision voltage (50 V, Figure 5A), whereas 2G12 I19R started to unfold at 70 V (Figure 5B). The second 2G12 unfolded intermediate was maintained to 120 V compared to 2G12 I19R which unfolded earlier (110 V). Consistent with Figure 2, the drift times of the initial folded state differed (2G12 I19R = 9.1 ms, 2G12 = 9.6 ms) but interestingly, the drift time of the second intermediate were similar for both Abs (~12.5 ms). This could be interpreted as both 2G12s un-folding towards a similar configuration or unfolding of the Fab domain during first transition. A third unfolded state was observed for the 24^+ with some low-intensity signal detected which may correspond to a fourth state (~16ms). The choice of charge state used for antibody CIU experiments has been previously described[34] and influences the amount and features of transitions. This differential behaviour between domain-exchanged and non-exchanged antibodies of the 24^+ charge state showed clear differences in gas-phase stability and unfolding existed between the two Ab forms. CIU experiments were performed using two biological replicates (two separate Ab expressions) for both 2G12 anti-bodies, and the root-mean-squared-deviation (RMSD) values were calculated using the CIUSuite software[37]. The RMSD values were 7.51% and 9.29% for 2G12 and 2G12 I19R respectively, suggesting minimal differences within each replicate[32]. The RMSD value for the difference plot was much greater (RMSD=25.28%) revealing the considerable differences between the two 2G12 Abs.

Glycosylation Analysis of 2G12 and 2G12 I19R

Antibody glycosylation has been shown to affect CIU fingerprinting of antibodies[32,34] and may account for different unfolding profiles observed for the 2G12-based architectures. Although 2G12 and 2G12 I19R differ by a single amino acid substitution, it is conceivable that Fc glycosylation may account for CIU discrepancies, yet any glycan-specific induced stability effects in the gas-phase is unclear. To confirm the glycosylation status of both 2G12 and 2G12 I19R, N-glycans were released by PNGase F digestion and analyzed by HILIC-UHPLC (Figure 6). UHPLC analysis of fluorescently labelled glycans provided relative amounts of each glycan and no major differences were observed between 2G12 antibodies. Both 2G12 and 2G12 I19R glycans were equivalent and also similar to typical IgG1s with the fucosylated a-, mono- and digalactosylated biantennary glycans being the most dominant[46]. However, 2G12 exhibited slightly more $Man_5GlcNAc_2$ glycan than 2G12 I19R but no previous influence on this glycan on CIU has been reported. Individual glycan structures were further characterized by IM-MS (Figure S1).

Collision Induced Unfolding of 2G12 and 2G12 I19R Fab and Fc domains

To confirm that the observations made from the CIU profiles in Figure 5 were solely due to the domain-exchanged architecture rather than other factors, an IgG degrading enzyme from *Streptococcus pyogenes* (IdeS) cleavage was used to isolate the two regions. IdeS specifically cleaves IgGs between the Fc and Fab at a single site at the lower hinge region leaving both fragments intact[48]. After incubation with IdeS, the Fab and Fc regions were unfolded as before, with the Fc domains of both 2G12 and 2G12 I19R unfolding in an identical manner (Figure 7). However, CIU of the Fab regions differed and were analogous to the intact CIU results. Overall three unfolded states were observed and the domain exchanged 2G12 Fab unfolded first (55V) whilst the 2G12 I19R Fab unfolded at a higher collision energy (70V). Unfolding to the third state occurred at 125V and 150V for 2G12 and 2G12 I19R, respectively. On the whole, CIU profiles of both the domain-exchanged intact antibody and isolated Fabs unfolded at lower collision voltages than the non-domain-exchanged IgGs.

Collision Induced Unfolding of 2G12 I19R is equivalent to standard IgG antibodies

To confirm that the CIU profiles of 2G12 I19R were consistent with other IgG1 antibodies, two representative antibodies were tested. The first is the well-known IgG1 therapeutic antibody, trastuzumab, and the other is an HIV-neutralising IgG1 antibody, b12[49,50] (Figure 8). The CIU profiles of the 24^+ charge state were similar with trastuzumab, b12 and 2G12 I19R unfolding first at a collision voltage of 70 V. The second transition occurred at a collision voltage of 120 V. The unfolding patterns of b12, trastuzumab and 2G12 I19R was observed across all other major charge states (22^+, 23^+, 25^+) (Figure S2) and differed to 2G12. As discussed above, charge state selection for CIU fingerprinting is an important factor when comparing antibodies.

CONCLUSIONS

Identification of Ab structural features has generally been approached by classical techniques including X-ray crystallography and electron microscopy. Further structural

details have been investigated using thermodynamic, hydrodynamic, scattering, and other spectroscopic and mass spectrometric methodologies. Here, we demonstrate that native mass spectrometry and collision-induced unfolding can complement these established methods by rapidly and sensitively distinguish between domain-exchanged and non-exchanged antibody architectures. We further demonstrate that the change in gas-phase unfolding is localized to Fab domains, identified specifically after IdeS cleavage. The characteristics of the full-length antibody CIU profiles are consistent between canonical IgG1 structures thereby providing a benchmark for screening for antibody features, including domain-exchanged architectures, extended CDRs, and potentially the correct assembly of multi-specific antibodies. The applications for CIU in characterisation of unusual antibody architectures offers the potential for this technique to become a high-throughput screening tool during the development of macromolecular drugs.

Supplementary Material

Refer to Web version on PubMed Central for supplementary material.

Acknowledgments

We kindly thank David Staunton for assisting in DSC measurements (University of Oxford, Department of Biochemistry, Bio-physics Facility). MC and WBS gratefully acknowledges a research grant from Against Breast Cancer (www.againstbreastcancer.org; UK Charity 1121258). MC was the Against Breast Cancer Fellow in Cancer Therapeutics at Oriel College, Oxford. MC is additionally supported by Scripps CHAVI-ID (grant 1UM1AI100663), which provided funds to purchase the Synapt G2Si mass spectrometer.

References

1. Ecker DM, Jones SD, Levine HL. mAbs. 2015; 7:9–14. [PubMed: 25529996]
2. Carter PJ, Lazar GA. Nat. Rev. Drug Discov. 2018; 17:197–223. [PubMed: 29192287]
3. Nelson AL, Dhimolea E, Reichert JM. Nat. Rev. Drug Discovery. 2010; 9:767–774. [PubMed: 20811384]
4. Sliwkowski MX, Mellman I. Science. 2013; 341:1192–1198. [PubMed: 24031011]
5. Blundell PA, Le NPL, Allen J, Watanabe Y, Pleass RJ. J. Biol. Chem. 2017; 292:12994–13007. [PubMed: 28620050]
6. Le NPL, Bowden TA, Struwe WB, Crispin M. Biochim. Biophys. Acta, Gen. Subj. 2016; 1860:1655–1668.
7. Li T, DiLillo DJ, Bournazos S, Giddens JP, Ravetch JV, Wang LX. Proc. Natl. Acad. Sci. U. S. A. 2017; 114:3485–3490. [PubMed: 28289219]
8. Jefferis R. J. Immunol. Res. 2016; 2016:5358272. [PubMed: 27191002]
9. Brinkmann U, Kontermann RE. mAbs. 2017; 9:182–212. [PubMed: 28071970]
10. Chames P, Baty D. mAbs. 2009; 1:539–547. [PubMed: 20073127]
11. Fan G, Wang Z, Hao M, Li J. J. Hematol. Oncol. 2015; 8:130. [PubMed: 26692321]
12. Calarese DA, Scanlan CN, Zwick MB, Deechongkit S, Mimura Y, Kunert R, Zhu P, Wormald MR, Stanfield RL, Roux KH, Kelly JW, Rudd PM, Dwek RA, Katinger H, Burton DR, Wilson IA. Science. 2003; 300 [PubMed: 12829775]
13. Scanlan CN, Pantophlet R, Wormald MR, Ollmann Saphire E, Stanfield R, Wilson IA, Katinger H, Dwek RA, Rudd PM, Burton DR. J. of Virol. 2002; 76:7306–7321.
14. Sanders RW, Venturi M, Schiffner L, Kalyanaraman R, Katinger H, Lloyd KO, Kwong PD, Moore JP. J. of Virol. 2002; 76:7293–7305.
15. Doores KJ, Fulton Z, Huber M, Wilson IA, Burton DR. J. of Virol. 2010; 84:10690–10699.

16. Dunlop DC, Bonomelli C, Mansab F, Vasiljevic S, Doores KJ, Wormald MR, Palma AS, Feizi T, Harvey DJ, Dwek RA, Crispin M, Scanlan CN. Glycobiology. 2010; 20:812–823. [PubMed: 20181792]
17. Scanlan CN, Pantophlet R, Wormald MR, Ollmann Saphire E, Stanfield R, Wilson IA, Katinger H, Dwek RA, Rudd PM, Burton DR. J. of Virol. 2002; 76:7306–7321.
18. Murin CD, Julien J-P, Sok D, Stanfield RL, Khayat R, Cupo A, Moore JP, Burton DR, Wilson IA, Ward AB. J. of Virol. 2014; 88:10177–10188.
19. Huber M, Le KM, Doores KJ, Fulton Z, Stanfield RL, Wilson IA, Burton DR. J. of Virol. 2010; 84:10700–10707.
20. Ehkirch A, D'Atri V, Rouviere F, Hernandez-Alba O, Goyon A, Colas O, Sarrut M, Beck A, Guillarme D, Heinisch S, Cianferani S. Anal. Chem. 2018; 90:1578–1586. [PubMed: 29260862]
21. Ferguson CN, Gucinski-Ruth AC. J. Am. Soc. Mass Spectrom. 2016; 27:822–833. [PubMed: 26988372]
22. Schachner L, Han G, Dillon M, Zhou J, McCarty L, Ellerman D, Yin Y, Spiess C, Lill JR, Carter PJ, Sandoval W. Anal. Chem. 2016; 88:12122–12127. [PubMed: 28193052]
23. Terral G, Beck A, Cianferani S. J. Chromatogr. B. 2016; 1032:79–90.
24. Pacholarz KJ, Peters SJ, Garlish RA, Henry AJ, Taylor RJ, Humphreys DP, Barran PE. Chembiochem. 2016; 17:46–51. [PubMed: 26534882]
25. Edgeworth MJ, Phillips JJ, Lowe DC, Kippen AD, Higazi DR, Scrivens JH. Angew. Chem., Int. Ed. Engl. 2015; 54:15156–15159.
26. Pacholarz KJ, Porrini M, Garlish RA, Burnley RJ, Taylor RJ, Henry AJ, Barran PE. Angew. Chem., Int. Ed. Engl. 2014; 53:7765–7769.
27. Gahoual R, Heidenreich AK, Somsen GW, Bulau P, Reusch D, Wuhrer M, Haberger M. Anal. Chem. 2017; 89:5404–5412. [PubMed: 28398745]
28. Pisupati K, Tian Y, Okbazghi S, Benet A, Ackermann R, Ford M, Saveliev S, Hosfield CM, Urh M, Carlson E, Becker C, Tolbert TJ, Schwendeman SP, Ruotolo BT, Schwendeman A. Anal. Chem. 2017; 89:4838–4846. [PubMed: 28365979]
29. Hopper JTS, Oldham NJ. J. Am. Soc. Mass Spectrom. 2009; 20:1851–1858. [PubMed: 19643633]
30. Huang YN, Salinas ND, Chen E, Tolia NH, Gross ML. J. Am. Soc. Mass Spectrom. 2017; 28:2515–2518. [PubMed: 28875466]
31. Wagner ND, Clemmer DE, Russell DH. Anal. Chem. 2017; 89:10094–10103. [PubMed: 28841006]
32. Tian Y, Han L, Buckner AC, Ruotolo BT. Anal. Chem. 2015; 87:11509–11515. [PubMed: 26471104]
33. Marcoux J, Champion T, Colas O, Wagner-Rousset E, Corvaia N, Van Dorsselaer A, Beck A, Cianferani S. Protein Sci. 2015; 24:1210–1223. [PubMed: 25694334]
34. Dixit SM, Polasky DA, Ruotolo BT. Curr. Opin. Chem. Biol. 2018; 42:93–100. [PubMed: 29207278]
35. Struwe WB, Stuckmann A, Behrens AJ, Pagel K, Crispin M. ACS Chem. Biol. 2017; 12:357–361. [PubMed: 27984693]
36. Allison TM, Reading E, Liko I, Baldwin AJ, Laganowsky A, Robinson CV. Nat. Commun. 2015; 6:1–10.
37. Eschweiler JD, Rabuck-Gibbons JN, Tian Y, Ruotolo BT. Anal. Chem. 2015; 87:11516–11522. [PubMed: 26489593]
38. Pritchard LK, Vasiljevic S, Ozorowski G, Seabright GE, Cupo A, Ringe R, Kim HJ, Sanders RW, Doores KJ, Burton DR, Wilson IA, Ward AB, Moore JP, Crispin M. Cell Rep. 2015; 11:1604–1613. [PubMed: 26051934]
39. Harvey DJ, Crispin M, Bonomelli C, Scrivens JH. J. Am. Soc. Mass Spectrom. 2015; 26:1754–1767. [PubMed: 26204966]
40. Behrens A-J, Vasiljevic S, Pritchard LK, Harvey DJ, Andev RS, Krumm SA, Struwe WB, Cupo A, Kumar A, Zitzmann N, Seabright GE, Kramer HB, Spencer DIR, Royle L, Lee JH, Klasse PJ, Burton DR, Wilson IA, Ward AB, Sanders RW, et al. Cell Rep. 2016; 14:2695–2706. [PubMed: 26972002]

41. Pritchard LK, Harvey DJ, Bonomelli C, Crispin M, Doores KJ. J. of Virol. 2015; 89:8932–8944.
42. Pritchard LK, Spencer DIR, Royle L, Bonomelli C, Seabright GE, Behrens A-J, Kulp DW, Menis S, Krumm SA, Dunlop DC, Crispin DJ, Bowden TA, Scanlan CN, Ward AB, Schief WR, Doores KJ, Crispin M. Nat. Commun. 2015; 6:1–11.
43. Ionescu RM, Vlasak J, Price C, Kirchmeier M. J. Pharm. Sci. 2008; 97:1414–1426. [PubMed: 17721938]
44. Ito T, Tsumoto K. Protein Sci. 2013; 22:1542–1551. [PubMed: 23963869]
45. Brader ML, Estey T, Bai S, Alston RW, Lucas KK, Lantz S, Landsman P, Maloney KM. Mol. Pharmaceutics. 2015; 12:1005–1017.
46. Stö H, Adamczyk B, Hayes J, Rudd PM. Anal. Chem. 85:8841–8849.
47. Guile GR, Rudd PM, Wing DR, Prime SB, Dwek RA. Anal. Biochem. 1996; 240:210–226. [PubMed: 8811911]
48. Akesson P, Moritz L, Truedsson M, Christensson B, von Pawel-Rammingen U. Infect. Immun. 2006; 74:497–503. [PubMed: 16369006]
49. Saphire EO, Parren PW, Pantophlet R, Zwick MB, Morris GM, Rudd PM, Dwek RA, Stanfield RL, Burton DR, Wilson IA. Science. 2001; 293:1155–1159. [PubMed: 11498595]
50. Zwick MB, Parren PWHI, Saphire EO, Church S, Wang M, Scott JK, Dawson PE, Wilson IA, Burton DR. J. of Virol. 2003; 77:5863–5876.

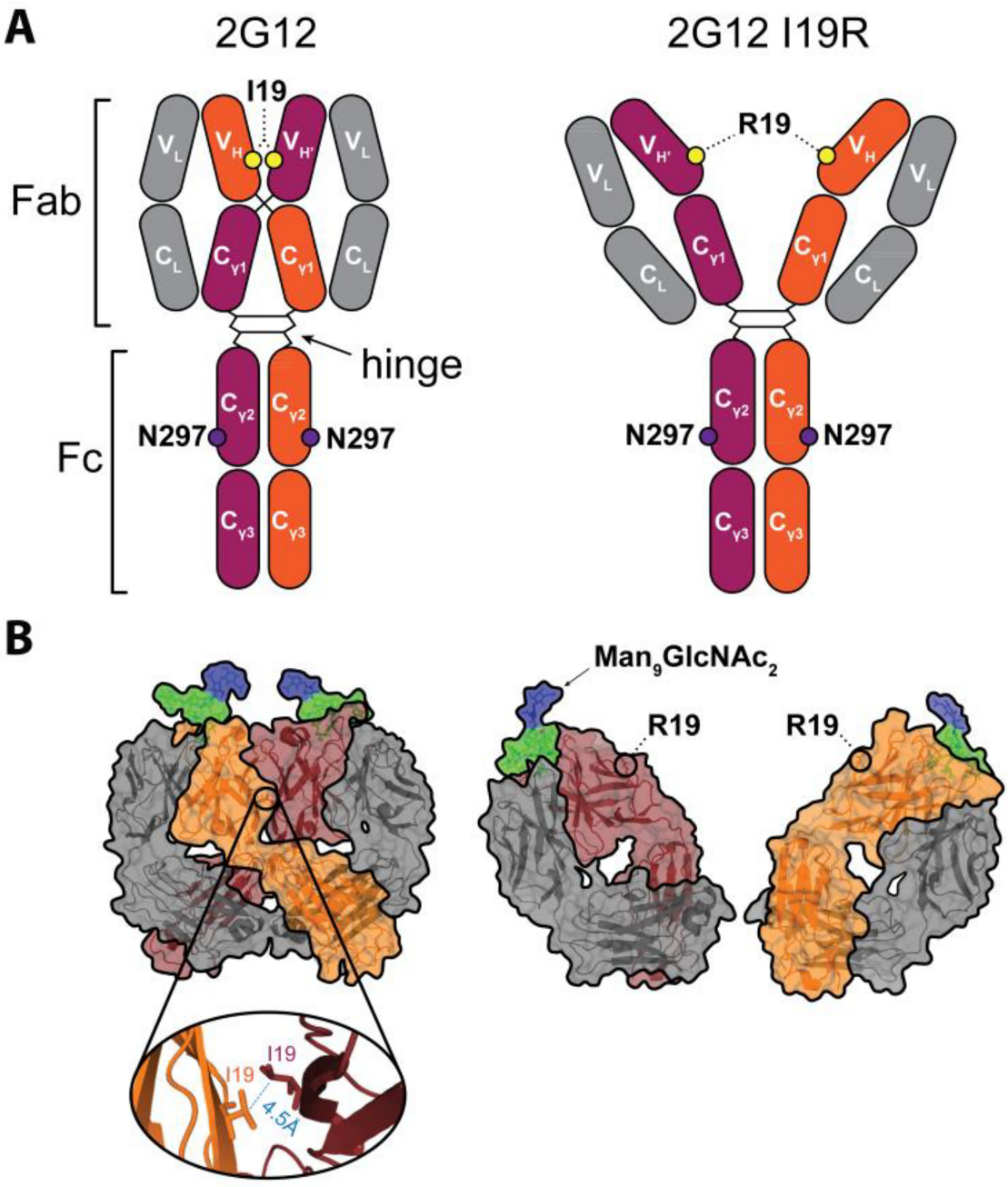

Figure 1.

(A) Cartoon structures of domain-exchanged 2G12 and 2G12 I19R antibodies showing the location of Fab, hinge and Fc regions (domains are labelled with white text). Light chains are grey and heavy chains are coloured dark red and orange. The location of amino acid I19/R19 on both heavy chains is labelled yellow and the conserved Asn297 N-linked glycosylation site is purple. **(B)** Crystal structures of 2G12 (PDB: 1OM3) and 2G12 I19R (PDB: 3OAU) Fab domains with a single $Man_9GlcNAc_2$ glycan bound to each antigen binding site. Mannose, green. GlcNAc, blue.

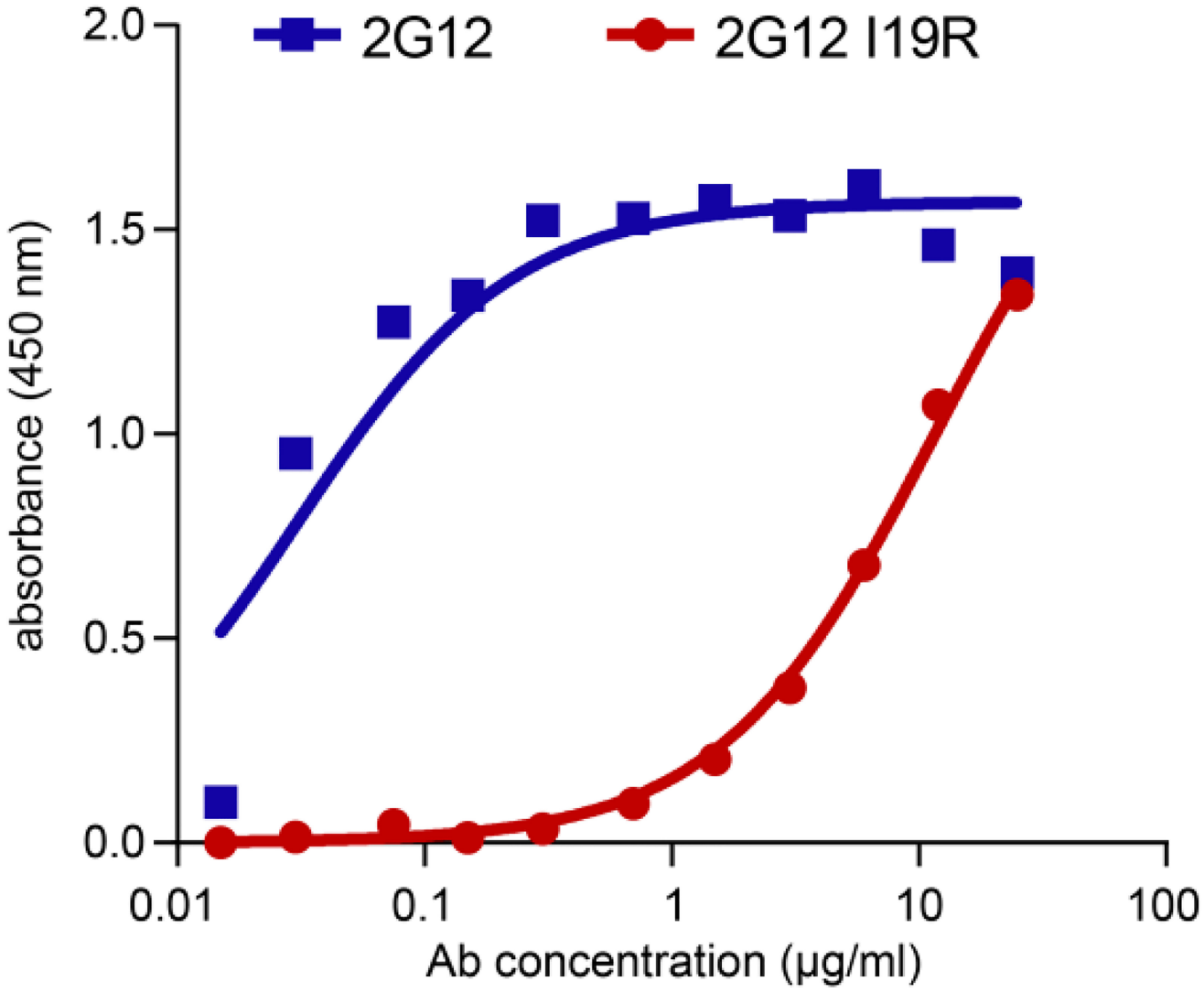

Figure 2.

Binding assay of 2G12 (blue) and 2G12 I19R (red) to recombinant HIV gp120. ELISAs were performed with Ni^{+} immobilised gp120 and serial Ab dilutions.

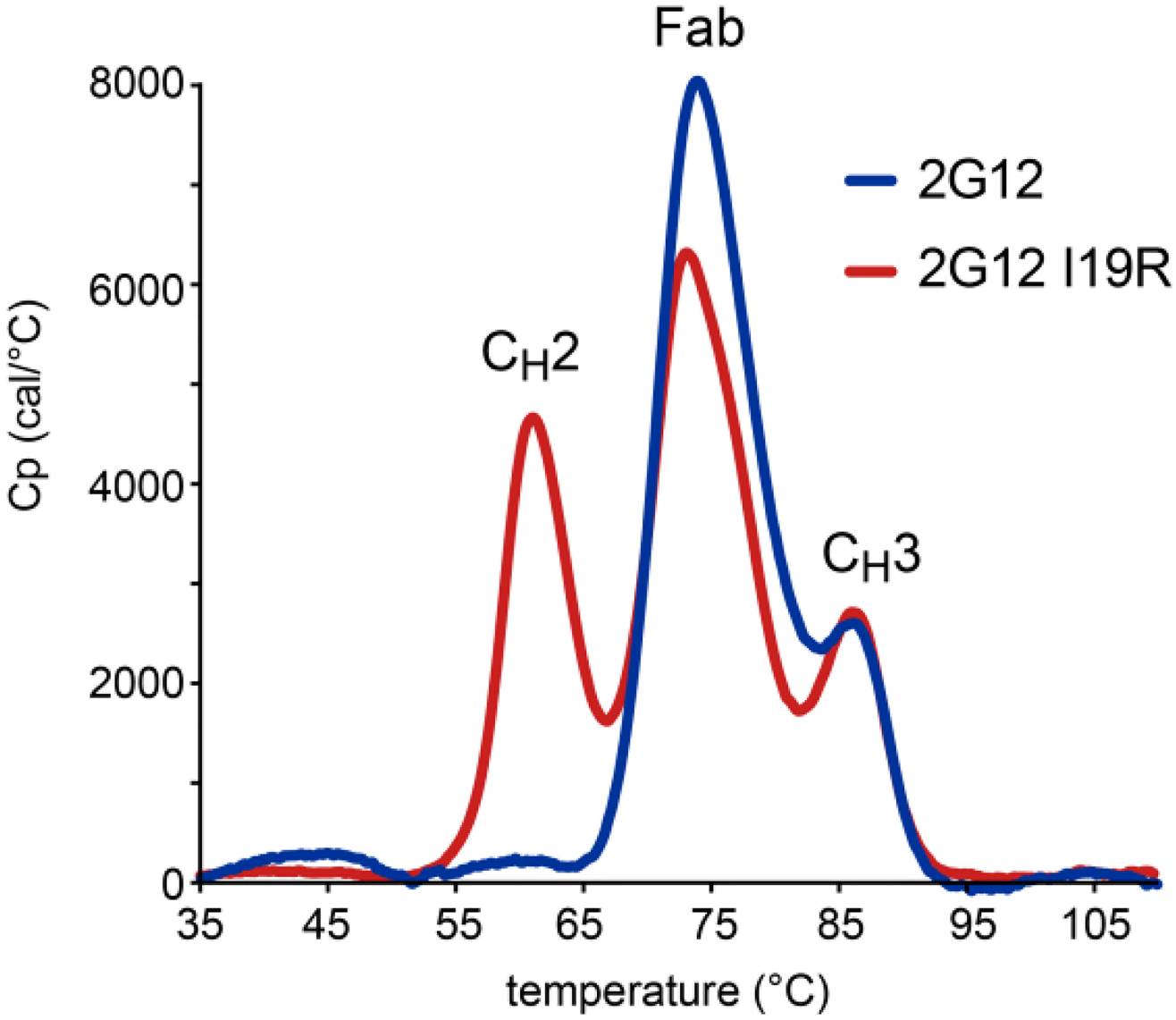

Figure 3.
Differential Scanning Calorimetry of 2G12 (blue) and 2G12 I19R (red). Cp, specific heat capacity. Peaks are labelled based on previously reported IgG1 assignments[43,44].

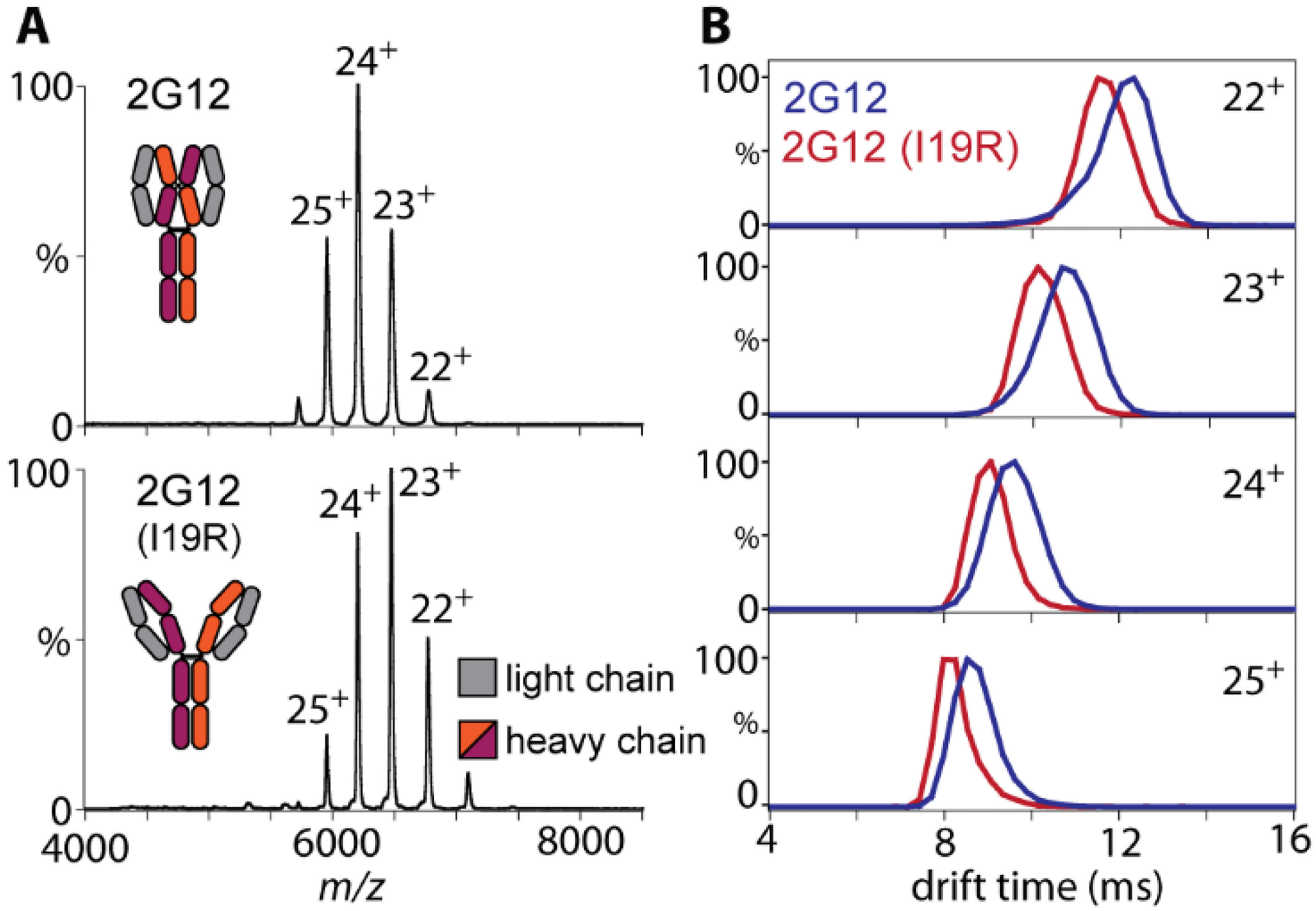

Figure 4.

(**A**) Native mass spectra of 2G12 and 2G12 I19R. (**B**) Arrival time distributions of 2G12 (blue) and 2G12 I19R (red) 22^+ to 25^+ charge states.

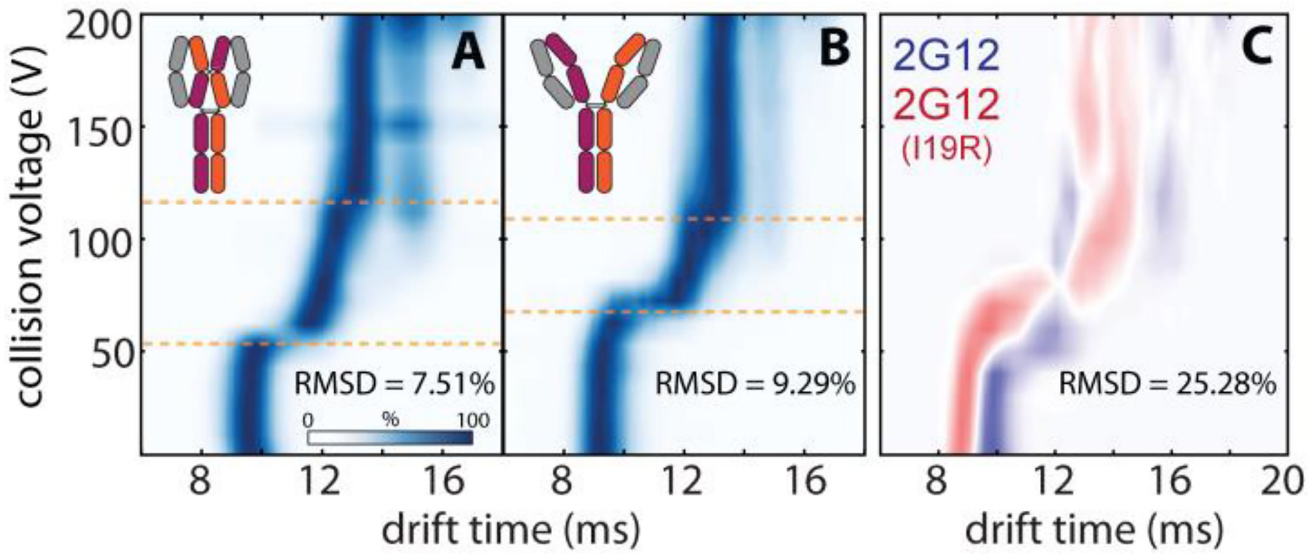

Figure 5.

Collision-induced unfolding profiles of the 24^{+} charge state of 2G12 (**A**) and 2G12 I19R (**B**). The orange dotted lines indicate the collision voltage at the two observed transition states. The blue gradient represents normalised ion intensities for each voltage scan. (**C**) Difference overlay of 2G12 (blue) and 2G12 I19R (red) CIU profiles.

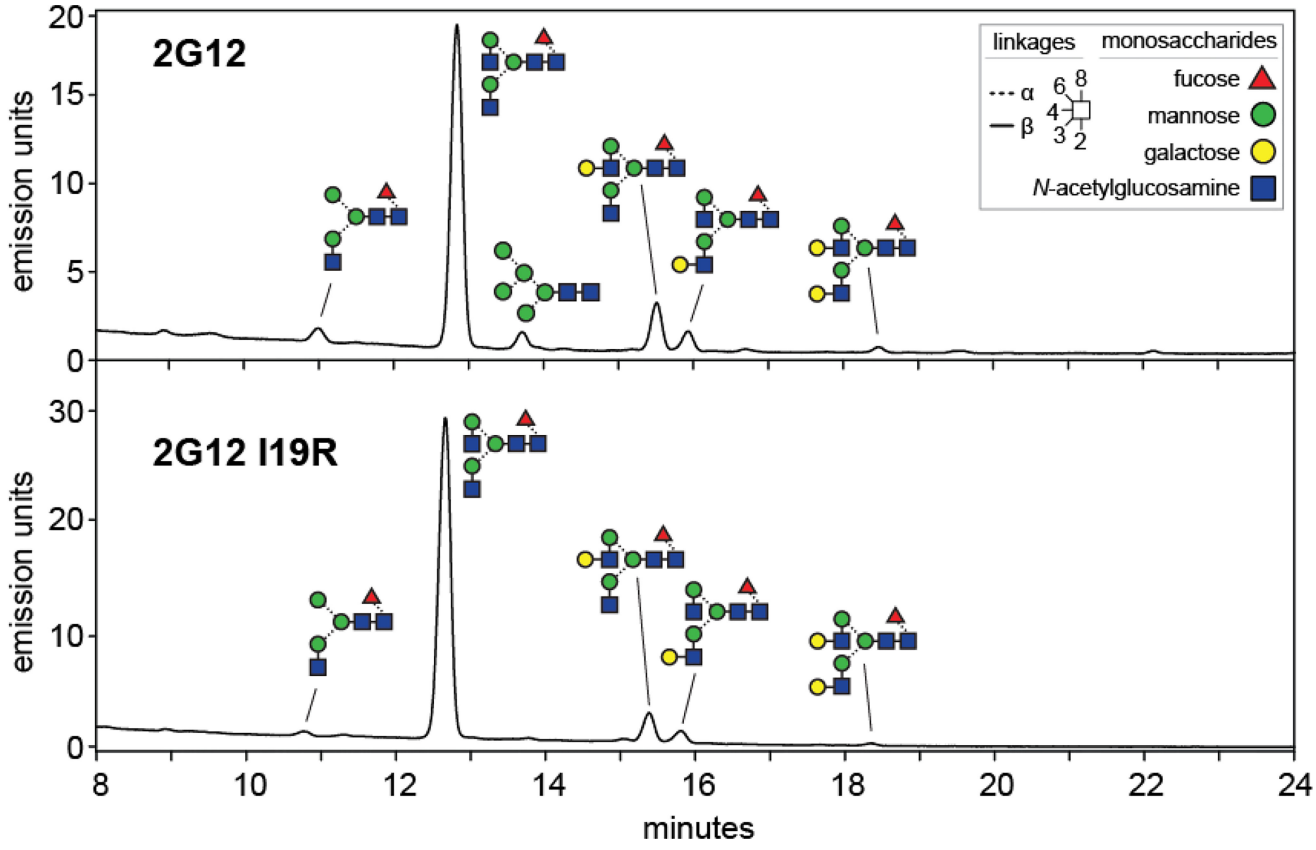

Figure 6.

Glycan analysis by HILIC-UHPLC of 2AA-labelled glycans from 2G12 and 2G12 I19R. Peaks were labelled accordingly to previous assignments[47].

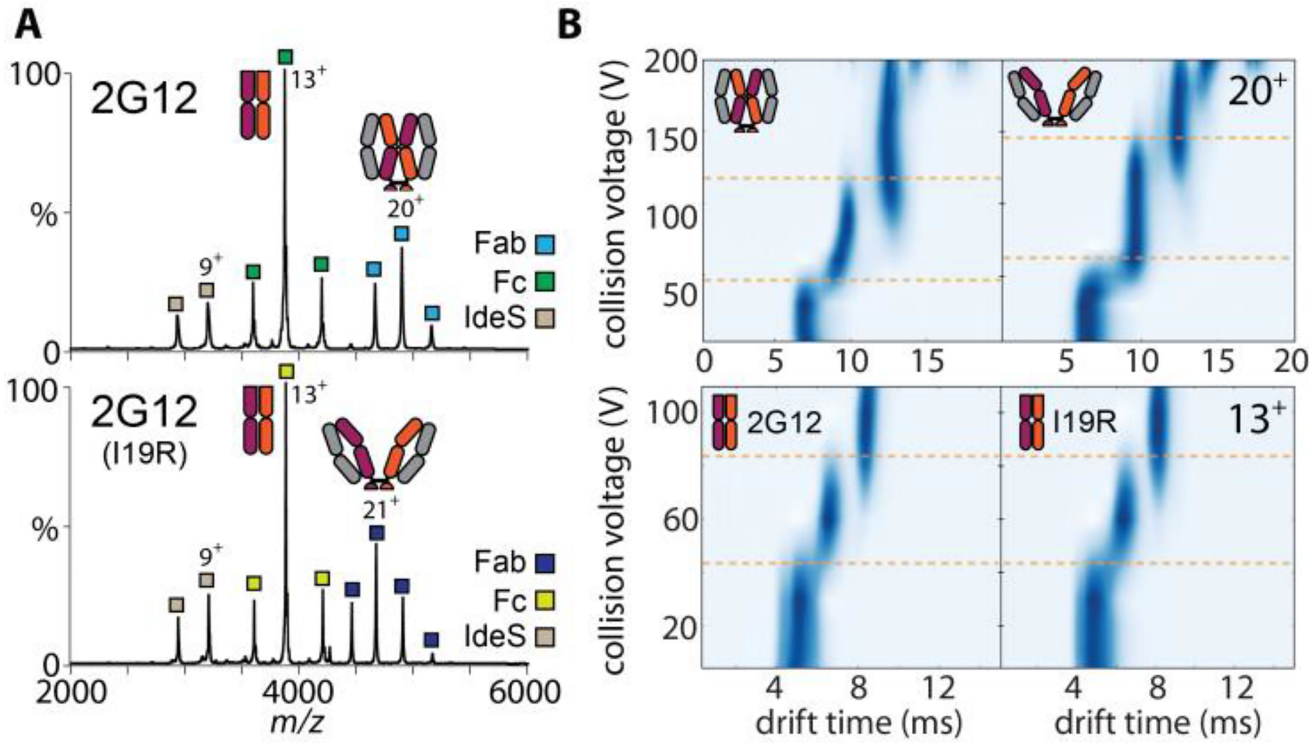

Figure 7.

(**A**) Native mass spectra of 2G12 and 2G12 I19R treated with IdeS. (**B**) Unfolding plots of 2G12 Fab domains (20^+ charge state) and Fc domains (13^+ charge state). The orange dotted lines indicate the collision voltage at each observed transition states.

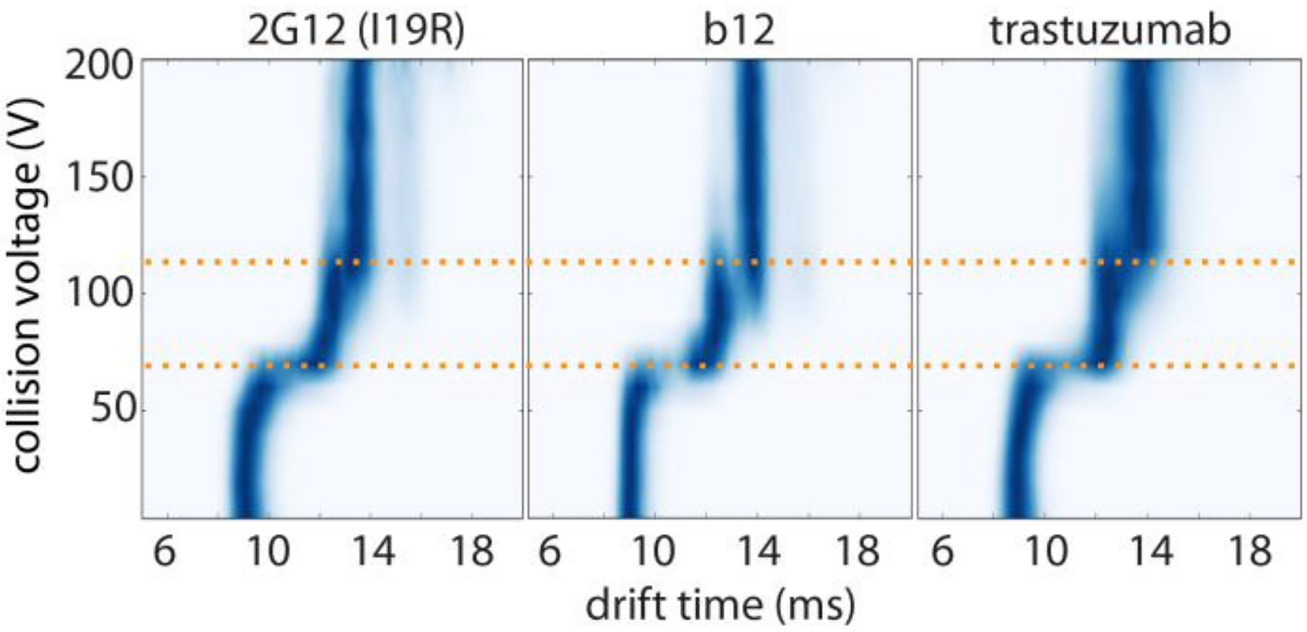

Figure 8.

Collision-induced unfolding profiles of conventional IgG1 antibodies b12 and trastuzumab alongside 2G12 I19R (24^+ charge state). The dashed orange lines represent the un-folding transitions.